

Instability of the kinematic state in the atmosphere of the hypergiant ρ Cas outside outburst

V.G. Klochkova¹, V.E. Panchuk¹, N.S. Tavganskaya¹, and I.A. Usenko²

1 – Special Astrophysical Observatory, Nizhnij Arkhyz, 369167, Russia

2 – Astronomical Observatory, Odessa National University, Odessa, 65014 Ukraine

April 30, 2018

Abstract Observations of the yellow hypergiant ρ Cas obtained in 2007–2011 in a wide wavelength region with spectral resolution $R \geq 60\,000$ have enabled studies of features of its optical spectrum in detail and brought to light previously unknown characteristics of the extended atmosphere of the star. The radial velocity measured from symmetric absorptions of metals varies with an amplitude of about ± 7 km/s around the systemic velocity $V_{\text{sys}} = -47$ km/s, due to low-amplitude pulsations of the atmospheric layers near the photosphere. At some times, a velocity gradient was found in deep atmospheric layers of the star. A slight velocity stratification in the stellar atmosphere was detected for the first time, manifested as a difference of 3–4 km/s in the velocities measured from absorption lines of neutral metals and of ions. The long-wavelength components of split absorptions of BaII, SrII, TiII, and other strong lines with low excitation potentials for their lower levels are distorted by nearby emission lines. It is suggested that the short-wavelength components, whose locations correspond to the narrow velocity range $V_r(\text{blue})$ from approximately -60 to -70 km/s, are formed in a circumstellar envelope; one component of the D NaI doublet and the emission components of the FeII 6369.46 and 6432.68 Å ions are also formed there.

Keywords: massive stars, evolution, hypergiants, envelopes, spectra.

1. Introduction

Yellow hypergiants – rare stars whose prototype is ρ Cas (Sp = G2 Iae) are evolved high-mass stars with super-high luminosities. Such objects are found near the luminosity limit on the Hertzsprung–Russell diagram, in the instability region containing hypergiants with spectral types from A to M [1, 2, 3]. The abundances of CNO elements and the sodium excess in the atmosphere of ρ Cas [4] indicate that the star has already passed the red-supergiant phase, and is now in a rapid evolutionary transition from a red supergiant to a Wolf–Rayet or LBV star. The process of this motion towards higher temperatures is poorly studied.

Apart from their high luminosities, yellow hypergiants differ from ordinary supergiants in their high mass-loss rates via their stellar winds and in the presence of circumstellar envelopes. The instability of these objects is also manifest through pulsation-type spectral and brightness variations. The characteristic features of the pulsations of massive stars at the stage of contraction of the helium core were considered by Fadeyev [5], who concluded that

long-period radial pulsations were improbable for ρ Cas. Along with the above manifestations of instability, yellow hypergiants also undergo so-called “shell episodes”, when the star loses matter especially efficiently and becomes enshrouded for several hundred days by the ejected cool matter, which forms a pseudo-photosphere. In the case of ρ Cas, the most recent event of this kind occurred in late 2000 – early 2001, when the star lost up to $3 \times 10^{-2} \mathcal{M}_{\odot}$ [6].

On the Hertzsprung–Russell diagram, ρ Cas is at the boundary of the so-called “yellow void” [1] separating hypergiants from LBV stars in quiescence. Hypergiants near the void exhibit negative density gradients and nearly-zero surface gravities $\log g$ [7], favoring the formation of an instability region in the atmosphere. The pulsation amplitudes of yellow hypergiants apparently strongly increases at the boundary of the yellow void, resulting in increased atmospheric instability and shell ejection [1].

Close to ρ Cas in the Hertzsprung–Russell diagram, we find the hypergiant V1302 Aql, better known as the associated IR–source IRC +10420. The central star of V1302 Aql (spectral type F8 Ia, luminosity of the order of $10^6 L_{\odot}$) is surrounded by a dense gas and dust medium, so that only the wind can be observed. Despite its fairly high effective temperature, the star is associated with a strong OH maser. One of the most important results from many-year studies of V1302 Aql is the discovery of a rapid growth of its effective temperature [8, 9]. Monitoring data from the last decades of the 20th century indicate an acceleration of this temperature increase [10]. In contrast to the hypergiant V1302 Aql, which has a massive and structured envelope, ρ Cas is point-like in observations. An envelope far from the star that would be detectable with the Hubble Space Telescope is not present in ρ Cas, providing evidence that the duration of the high mass-loss stage has been short [11]. The peculiarity of ρ Cas and its spectral variations were detected more than a century ago (cf. [12] and references therein); however we still do not have a complete understanding of the physical processes resulting in the complex, time-variable kinematic situation in the extended atmosphere of this hypergiant. Fadeyev [5] notes that even the pulsation type remains unclear, making monitoring important.

Our two decade of spectroscopic monitoring of the hypergiant V1302 Aql with the 6-m telescope of the Special Astrophysical Observatory enabled us to draw conclusions concerning its evolution [8, 10]. The similarity of the evolutionary stage and fundamental parameters of V1302 Aql to those of ρ Cas stimulated monitoring for the latter rare yellow hypergiant. The current paper presents the results of our optical spectroscopic observations of ρ Cas performed in 2007–2011. Section 2 briefly describes the observations and data analysis. Section 3 presents our results and compares them to those published earlier. Our main conclusions are given in Section 4.

2. Observations, reduction, and spectral analysis

Spectroscopic observations of ρ Cas were carried out at the Nasmyth focus of the 6-m telescope using the NES echelle spectrograph [13, 14]. The mean epochs of our observations (JD) and the recorded spectral ranges are listed in Table 1. The observations were performed using a 2048×2048 pixel CCD chip and an image slicer [14]. A $2K \times 4K$ CCD chip was used on September 14, 2011. Table 1 shows that this transition to a large-format CCD considerably expanded the recorded wavelength range, $\Delta\lambda$. The spectroscopic resolving power was $\lambda/\Delta\lambda \geq 60000$, with the signal-to-noise ratio $S/N \geq 100$.

The one-dimensional spectra were extracted from the two-dimensional echelle frames using the modified [15] ECHELLE routine of the MIDAS software package. To remove cosmic-ray traces, we applied median averaging of two spectra taken just after one another. Our wavelength calibration was done using spectra from a Th Ar hollow-cathode lamp. We checked

Table 1. Log of observations of ρ Cas and the effective temperatures T_{eff} derived for various dates

Spectrum No.	Date	JD 2450000+	$\Delta\lambda$, Å	T_{eff} , K
s493015	09.03.2007	4168.63	4557–6014	6221±90
s494023	10.03.2007	4169.57	4557–6014	6200±171
s495019	10.03.2007	4170.49	4514–5940	6229±131
s516015	21.02.2008	4518.39	5204–6680	6610±53
s525032	19.10.2008	4759.23	3050–4520	
s526006	20.10.2008	4760.23	5214–6690	6744±53
s538009	30.09.2009	5104.62	5216–6691	6420±39
s553018	01.08.2010	5409.52	4422–5930	5777±161
s554032	23.09.2010	5463.39	3970–5390	
s555027	24.09.2010	5464.39	5216–6690	6044±40
s564020	13.01.2011	5574.60	5208–6683	6174±43
s565003	13.01.2011	5575.09	5208–6683	6322±52
s575002	14.09.2011	5819.41	3985–6980	

the instrumental agreement between the stellar and hollow-cathode lamp spectra using O_2 and H_2O telluric lines. To check the derived V_r values, we measured 15–20 telluric lines in the spectra of ρ Cas with their long-wavelength end at 5930–6010 Å and up to 70–80 lines in spectra with longer-wavelength ends. The rms uncertainty in the V_r measurements of narrow telluric absorption lines is ≤ 0.5 km/s (the uncertainty for a single line). The accuracy is somewhat poorer in the case of ρ Cas, since the spectral lines are broadened by turbulence: the microturbulence velocity in the atmosphere reaches 11 km/s [1]. The techniques used for the V_r measurements derived from spectra taken with the NES spectrograph, their uncertainties, and the sources of these uncertainties are described in more detail in [16, 17].

3. Main results

4. Effective temperature of ρ Cas

We determined the effective temperature, T_{eff} , using the spectroscopic criteria developed by Kovtyukh [18]. This method is based on ratios of selected spectral lines that are sensitive temperature indicators. A single pair of lines provides temperature with an uncertainty of 50–110 K, but using a set of criteria results in a fairly accurate mean value. We are able to use more than 100 line pairs in spectra of F–G stars, making it possible to reach an internal accuracy of 10–30 K. Table 1 shows that, due to the large line widths in the case of ρ Cas, our uncertainty is 39–53 K for the spectra in the range 5200–6700 Å. Due to a smaller number of available line pairs at ≈ 4400 –6020 Å the accuracy is poorer in this range: 90–170 K. Table 1 shows that the effective temperature varied during our observations in the range 5777–6744 K, with the mean being about 6200 K. The temperature variations we detected for ρ Cas in the course of its pulsation period exceed the temperature difference $\Delta T_{\text{eff}} \approx 750$ K obtained earlier by Lobel et al. [19].

Peculiarity and profile variations of spectral features

The profiles of strong absorption lines in the spectrum of ρ Cas are variable and, as a rule, asymmetric: their short-wavelength wings are either raised above the continuum by vari-

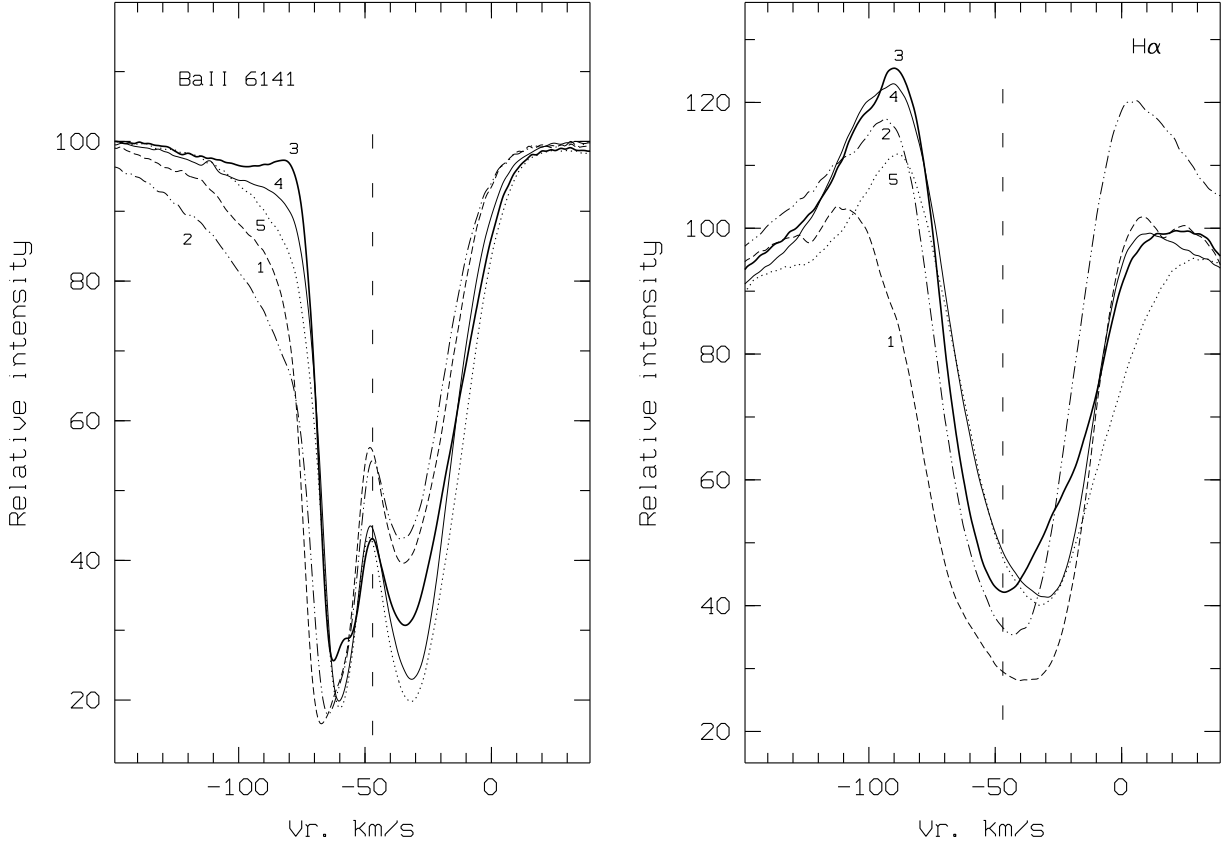


Figure 1. BaII 6141 Å profile and the central part of the H α profile in the spectra of ρ Cas for different epochs: 1 – February 21, 2008, 2 – October 20, 2008, 3 – September 30, 2009, 4 – September 24, 2010, 5 – January 13, 2011. The vertical dashed line indicates the systemic velocity, $V_{\text{sys}} = -47$ km/s [20, 19].

able emission or are more extended compared to the long-wavelength wing. A good example is the profile of the BaII 6141 Å line presented in the upper panel of Fig 1, which plots the residual intensity vs. the heliocentric radial velocity V_r . The short-wavelength wing of the BaII 6141 Å line, which forms in upper atmospheric layers under the influence of the stellar wind, sometimes attains values near -120 km/s, even reaching -170 km/s on October 20, 2008. Variations in the extended short-wavelength wings reflect kinematic instability in the upper levels of the atmosphere, which are subject to influence of the stellar wind.

In addition to extended short-wavelength wings, the strongest absorption lines in the spectra of ρ Cas also feature a peculiarity in their cores, which are permanently split into two components. The splitting of strong low-excitation absorption lines in the spectrum of ρ Cas has been known for a long time (cf. references in [20]). More than half a century ago, Sargent [21] presented a long list of such spectroscopic features. The wide spectral range recorded by us enabled us to identify 10–12 split absorption lines in the visible range, and more than 100 in the extended wavelength range, at $\lambda > 3500$ Å. A list of split absorption lines with the most trustworthy positions at $\lambda > 3900$ Å is presented in Table 2. Numerous split features are also present in the shorter wavelength range, $\lambda = 3500$ – 3900 Å, but their measurements are hindered by the fact that the spectrum is rich with blends. The lines with wavelengths longer than 5100 Å were already listed by Sargent [21]; the shorter-wavelength split absorption lines in the spectrum of ρ Cas were identified by us. We consider possible origin of this splitting in the next section, which deals with our analysis of the velocity field.

Our recorded spectral range contains the $H\alpha$ line at six epochs. The complex absorption and emission $H\alpha$ profile varies in time: the lower panel of Fig. 1 demonstrates that the position of the absorption core, intensities of the emission components, and their intensity ratios are all time variable. The varying position of the $H\alpha$ absorption core indicates that its formation region moves in the stellar atmosphere. Note that the displacement of the $H\alpha$ core during our observations was ≈ 16 km/s, while the earlier observations by Lobel et al. [19] detected core displacements as large as 35 km/s. No strict correlation is observed in the evolution of the $H\alpha$ and $BaII$ 6141 Å profiles.

It was proposed in [22] that the $H\alpha$ emission was formed in outer atmospheric layers that are thermally excited by shock waves. The emission is formed in thin high-temperature layers behind the shock front. Recombination occurs at this location, and the resulting emission lines should be seen against the absorption profile when the amount of hydrogen ionization due to the passage of the shock becomes high enough. The amount of ionization is related to the velocity of the shock. Note that the shock velocities that must be provided for Balmer emission to appear are much higher than the velocities observed for ρ Cas. In a model with a single shock, there is a slight velocity gradient in the recombination region, which determines the width of the emission line (taking into account integration across the visible hemisphere). It is emphasized in [22] that the cases when the emission line width is determined by thermal motions in a single high-temperature region and by several recombination regions formed at the boundary of each turbulent element cannot be distinguished spectroscopically. For this reason, the assumed turbulence spectrum is of key importance for explaining the observed microturbulence velocity, 11 km/s.

Another effect whose explanation requires the assumption of an ensemble of shocks with recombination is the long-lived, virtually permanent, presence of emission features. For example, a high optical depth of the heated layer in the $L\alpha$ line was used in [23] to explain the long-lived presence of Balmer emission in Mira stars. It is noted in [24] that it is difficult to explain long-lived Balmer emission in models with a shock emerging in the atmosphere, since the high-temperature region is quickly cooled by free-free transitions. Thus, the assumption of multiple shocks [22] is also required to explain the long duration of this emission. However, if indeed the observed line splitting is due to an emission component that “pushes apart” the remnant of a broad absorption line, we obtain an additional question: what is the excitation mechanism for the selected bound-bound transitions? We will consider the multipleshock hypothesis further in a special study.

We noted in the Introduction the similarity of the fundamental parameters and evolutionary stages for the two cool hypergiants ρ Cas and V1302 Aql. However, the two stars also have important differences. The first is the mass-loss rate: for V1302 Aql, this is $3 \div 6 \times 10^{-4} \mathcal{M}_{\odot}/\text{year}$, with possible episodes of increase to $10^{-3} \mathcal{M}_{\odot}/\text{year}$ (see [25] and references therein). This is one to two orders of magnitude higher than the upper limit for the mass-loss rate of ρ Cas, $9.2 \times 10^{-5} \mathcal{M}_{\odot}/\text{year}$ [19]. The high mass-loss rate of V1302 Aql has resulted in the formation of the powerful, structured circumstellar envelope observed by the Hubble Space Telescope [25]. The presence of this envelope produces a large IR-excess, making V1302 Aql a bright IR-source. The IR-fluxes of this star in the IRAS bands are higher than those of ρ Cas by a factor of 40–50. Despite the similarity of their MK spectral types, the optical spectra of the two hypergiants are also considerably different. Permitted and forbidden emission lines, often with intensities exceeding those of the local continuum by large factors, dominate the spectrum of V1302 Aql. The HI and $CaII$ line profiles are two-peaked, and lines of metal ions often possess P Cygni profiles [8, 9, 10]. The spectrum of ρ Cas resembles that observed for V1302 Aql in the 1970s [26]: it is close to that of a normal F-supergiant, with a modest addition of some emission features. The main differences from

the spectra of normal supergiants are its broader absorption lines, due to very high luminosity and well-developed atmospheric turbulence, and the splitting of the strongest metal absorption lines.

Velocity field in the atmosphere and envelope of ρ Cas

The systemic velocity of ρ Cas

Lambert et al. [20] used observations of the IR spectrum of ρ Cas to determine the heliocentric systemic velocity, $V_{\text{sys}} = -48 \pm 2$ km/s. Lobel et al. [27] used the systemic velocity $V_{\text{sys}} = -42$ km/s, while a later paper of Lobel et al. [19] assumes $V_{\text{sys}} = -47 \pm 1$ km/s. We have adopted $V_{\text{sys}} = -47 \pm 1$ km/s, in agreement with the results of [19]. Note that the membership of ρ Cas in the stellar association Cas OB5 suggests the mean velocity of a sample of 21 stars in the association, $V_{\text{ass}} = -44.5$ km/s [28] for the systemic velocity of ρ Cas.

The radial velocity from symmetric absorption lines.

Lobel et al. [6] monitored the radial velocity of ρ Cas using narrow fragments, 45 \AA wide, centered at 5187 \AA . We analyzed the velocity field in the atmosphere of ρ Cas using large numbers of individual spectral features, a fundamental difference from the approach used in [6]. Our wide wavelength range and the high accuracy of our velocity measurements from individual lines enabled us to study the velocity field using an unprecedentedly large number of isolated single lines (several hundred in each of the spectra), as well as split lines.

Components of split absorption lines.

The second group of lines are the short-wavelength components of split low-excitation absorption lines. A list of split absorption lines in the spectra of ρ Cas is presented in Table 2. The identification and wavelengths follow the data of the spectroscopic atlas [29]; lower-level excitation potentials were taken from the VALD database [30, 31].

The fourth column of Table 3 contains the velocity $V_r(\text{blue})$ averaged for lines of a given group for each date. Three important points should be noted. First, the widths of the short-wavelength components are smaller than those of the long-wavelength components, and their unblended left wings have steeper gradients than do the right wings of the long-wavelength components. This is clearly visible in the BaII 6141 \AA profile shown in the upper panel of Fig. 1. Second, the positions of the short-wavelength components are close to the CO line core in the near-IR [20, 32]. Obviously, the CO lines of an F-star can be formed only in the circumstellar envelope. Third, Fig. 2 shows that the velocity of the short-wavelength components $V_r(\text{blue})$ is not constant. It follows from Table 3 and Fig. 2 that the velocity of the envelope layers where the envelope absorption lines are formed varies in time in a narrow range, from -59.6 to -67.3 km/s. The temporal variations of the short-wavelength wings of these components (see the profiles of the BaII 6141 \AA line in Fig. 1 and of the NaI 5889 \AA line in Fig. 5) could be due to changes in the wind parameters.

Table 2: List of split lines in the spectra of ρ Cas

Element	λ , \AA	χ_{low} , eV
TiII	3913.47	0.95
FeI	3920.26	0.97
FeI	3922.91	0.97

Tabl. 2, continuation		
YII	3950.36	0.90
FeI	4005.24	1.56
TiII	4012.38	0.57
MnI	4030.75	0.00
MnI	4033.06	0.00
MnI	4034.48	0.00
FeI	4045.81	1.48
FeI	4063.59	1.56
FeI	4071.74	1.61
SrII	4077.71	0.00
FeI	4132.06	1.61
FeI	4143.87	1.56
FeI	4202.03	1.48
SrII	4215.52	0.00
CaI	4226.73	0.00
ScII	4246.82	0.32
FeI	4250.79	1.56
FeI	4271.76	1.48
FeI	4294.12	1.48
TiII	4300.04	1.18
FeI	4307.90	1.56
FeI	4325.76	1.61
TiII	4330.70	1.18
TiII	4337.91	1.08
FeI	4383.54	1.48
TiII	4395.03	1.08
FeI	4404.75	1.56
ScII	4415.55	0.60
TiII	4417.71	1.16
FeI	4427.31	0.05
TiII	4443.80	1.08
FeI	4461.65	0.08
TiII	4468.51	1.13
TiII	4501.27	1.12
TiII	4533.96	1.24
TiII	4549.62	1.58
BaII	4554.03	0.00
TiII	4563.76	1.22
TiII	4571.97	1.57
BaII	4934.08	0.00
TiII	5129.16	1.89
FeII	5169.03	2.89
MgI	5172.70	2.71
MgI	5183.62	2.71
FeI	5269.54	0.85
FeI	5328.04	0.92
FeI	5371.49	0.96
FeI	5397.13	0.92

Tabl. 2, continuation		
FeI	5405.77	0.99
FeI	5429.70	0.96
FeI	5434.52	1.01
FeI	5446.92	0.99
FeI	5455.62	1.01
BaII	5853.67	0.60
BaII	6141.71	0.70
BaII	6496.90	0.60

Vr values measured from emission and absorption lines in the spectrum of ρ Cas exhibit a large scatter, from -10 to -70 km/s. However, it follows from Fig. 2, which displays the dependence of the heliocentric radial velocity Vr on the depth of the corresponding line, that the velocities measured for each of the dates contain several fairly well isolated groups of lines. The radial velocities measured for ρ Cas from these line groups and for our observing epochs are presented in Table 3. The numbers of lines used to determine the mean velocity Vr for each of the groups are given in brackets. The first group includes the vast majority of all spectral lines: isolated symmetric lines of metals that are weak or have moderate intensity. The mean values corresponding to the positions of such absorption lines, Vr(sym), is given in the third column of Table 3. It follows from this table and Fig. 2 that the velocity Vr(sym), reliably measured from a large number of symmetric absorption lines, does not coincide with the systemic velocity, and varies from epoch to epoch in the range from -39.6 to -55.4 km/s. The mean value, Vr(sym) = -46.7 km/s, coincides with Vsys. These variations reflect pulsation motions in layers close to the photosphere, with an amplitude of several km/s around the systemic velocity.

Our position measurements for symmetric absorption lines also show a relation between Vr and line depth on individual observing dates, indicating the presence of a velocity gradient in the atmosphere of the star (see, for example, data for the spectra taken on September 30, 2009 and September 24, 2010). In addition, a difference by 3–4 km/s for velocities measured from absorption lines of neutral atoms and ions was found for some dates. This is observed for the spectra taken on February 21, 2008 and in 2010 as well as for both spectra of January, 2011. Thus, besides the earlier known pulsational variations, we found a weak stratification of the velocity field in the atmosphere of ρ Cas. The difference between the velocities measured from absorption lines of neutral atoms and ions reflects inhomogeneities in the outer atmospheric layers of the star. The detected differential line shifts vary in time, hindering a simple averaging of the velocities from arbitrary groups of absorption lines. It is obviously necessary to study the velocity field using homogeneous groups of spectral features, preferably those having similar intensities and ionization stages.

In addition, there is a slight velocity gradient at some epochs: Vr(blue) changes by 5–6 km/s from shallower to the deepest layers. The velocity gradient for the short-wavelength components of the split absorption lines increases the uncertainty of the mean Vr(blue) values (Table 3, the fourth column). Note that the velocity derived from the CO profile, which is formed in the uppermost layers of the envelope, continues the trend for increasing envelope expansion velocity shown by the strong absorption lines.

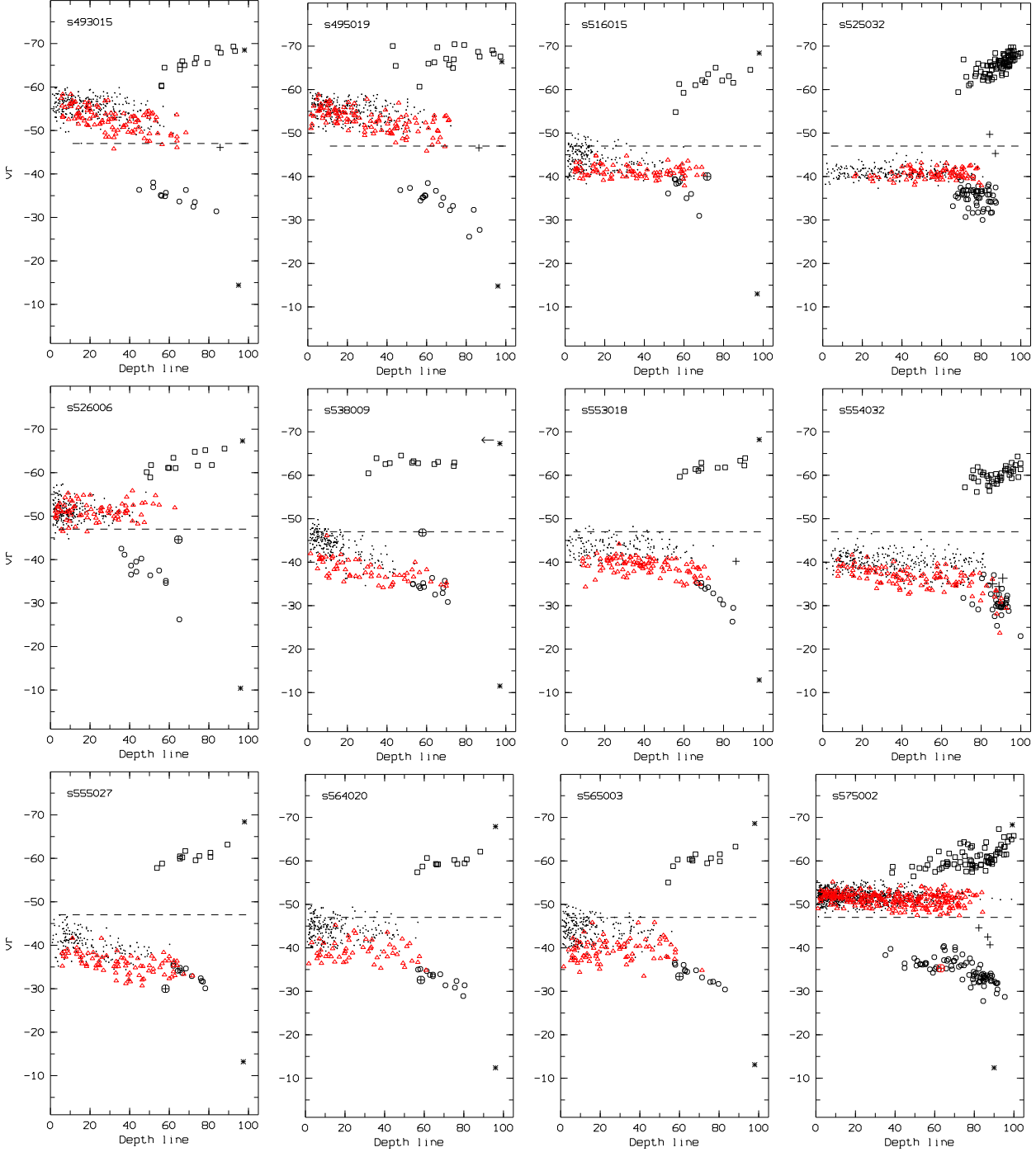


Figure 2. The radial velocity V_r measured from the absorption cores as a function of the line depth. The points are data for isolated symmetric absorption lines, the triangles data for absorption lines of ions, the squares and circles data for the short-wavelength and long-wavelength components of split absorption lines, the crosses data for absorption components of HI lines (the $H\alpha$ line can be identified as the circled cross), and the asterisks data for short-wavelength and long-wavelength components of the DNaI lines. The dashed line indicates the systemic velocity, $V_{\text{sys}} = -47$ km/s [19, 20]. The arrows in the panel for the spectrum s538009 mark the velocity from the FeII 6369.46 and 6432.68 Å emission components.

We are the first to detect a velocity gradient in the envelope. The possible presence of a gradient in the outflow velocity was noted by Sargent [21]. Later, Lambert et al. [20] used the

Table 3. Heliocentric radial velocities of ρ Cas. Vr(sym) is the mean velocity from symmetric absorption lines; Vr(blue) and Vr (red) are the mean velocities from the short-wavelength and long-wavelength components of split absorptions. The number of lines used to determine the mean values is in brackets; the last column contains the Vr(HI_abs) velocity measured from neutral-hydrogen absorption cores

Spectrum	Date	Vr, km/s			
		sym	blue	red	HI_abs
s493015	09.03.2007	-55.1 ± 0.09 (290)	-65.5 ± 0.4 (12)	-34.9 ± 0.4 (12)	-46.5^1
s494023	10.03.2007	-55.4 ± 0.10 (228)	-66.9 ± 0.4 (16)	-35.0 ± 0.4 (16)	-47.4^1
s495019	10.03.2007	-55.0 ± 0.09 (296)	-67.3 ± 0.4 (17)	-34.1 ± 0.4 (16)	-46.3^1
s516015	21.02.2008	-44.0 ± 0.11 (217)	-61.7 ± 0.5 (12)	-37.3 ± 0.5 (11)	-40.0^2
s525032	19.10.2008	-40.9 ± 0.07 (259)	-65.8 ± 0.1 (89)	-34.4 ± 0.2 (83)	$-49.1^3, -45.5^4$
s526006	20.10.2008	-51.1 ± 0.09 (235)	-62.2 ± 0.4 (12)	-37.1 ± 0.5 (12)	-44.6^2
s538009	30.09.2009	-43.6 ± 0.11 (220)	-62.8 ± 0.3 (12)	-34.3 ± 0.4 (12)	-46.2^2
s553018	01.08.2010	-43.4 ± 0.11 (170)	-61.8 ± 0.3 (11)	-32.6 ± 0.3 (11)	-40.2^1
s554032	23.09.2010	-39.6 ± 0.08 (333)	-60.0 ± 0.2 (41)	-30.0 ± 0.3 (34)	$-36.4^1, -36.4^3, -35.0^4$
s555027	24.09.2010	-40.2 ± 0.12 (173)	-60.3 ± 0.4 (11)	-33.4 ± 0.4 (12)	-30.2^2
s564020	13.01.2011	-44.0 ± 0.10 (235)	-59.6 ± 0.3 (11)	-32.9 ± 0.4 (12)	-32.6^2
s565003	13.01.2011	-43.9 ± 0.10 (249)	-60.1 ± 0.4 (12)	-33.9 ± 0.4 (12)	-33.4^2
s575002	14.09.2011	-51.8 ± 0.04 (934)	-60.7 ± 0.2 (76)	-34.8 ± 0.2 (82)	$-52.9^1, -29.8^2, -54.4^3, -49.4^4$

Vr from neutral-hydrogen absorption cores: ¹ – $H\beta$, ² – $H\alpha$, ³ – $H\delta$, ⁴ – $H\gamma$.

possible presence of a velocity gradient in the stellar envelope to explain the asymmetry of the CO profile.

The third group of lines is comprised of the long-wavelength components of split absorption lines. Figure 2 shows that, for most of these spectra, the dependence of Vr on the line depth is a continuation of the relations plotted for symmetric absorption lines. Note that the uncertainties of the mean velocities are much higher for the long-wavelength (Table 3, fifth column) than for the short-wavelength components. This is probably due to the complex character of the profiles of the long-wavelength components. We consider this in more detail below.

Lambert et al. [20] noted that the profiles of resonance (and strongest subordinate) photospheric absorption lines in the spectrum of ρ Cas were complex as early as 1981. We also believe that the long-wavelength components of the split absorption lines are ordinary strong absorption lines formed in high atmospheric layers. Their radial velocities differ from those of the high-intensity, isolated absorption lines due to the velocity gradient, as well as those of stationary emission lines formed in the circumstellar medium. The circumstellar emission lines, whose positions in the spectrum of ρ Cas do not coincide with the systemic velocity, exceed the local continuum level during outburst [6]. For observations outside outburst, the emission lines are weak, but they distort the long-wavelength components, shifting their cores toward longer wavelength. Figure 3 presents the profiles of several absorption lines with different intensities in the spectrum obtained on September 24, 2010 by way of illustration. The positions of absorption cores with low (FeI 6462 Å) and moderate intensity (SiII 6347 Å) correspond to the mean velocity for this epoch, Vr(sym) = -40 km/s from Table 3. At the same time, the core of the strong BaII 6141 Å line is shifted by approximately $+8$ km/s with respect to the relatively weak absorption lines.

Figure 4 compares a fragment of the observed (September 24, 2010) and synthetic spectra containing absorption lines with various intensities, including the split BaII 6141 Å line. The

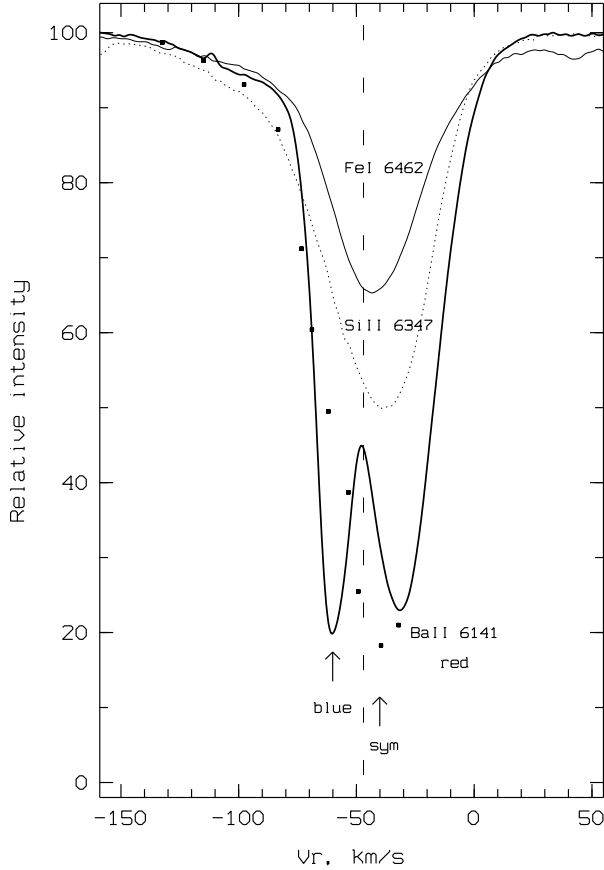


Figure 3. FeI 6462 Å, line profiles in the spectrum of ρ Cas obtained on September 24, 2010. The vertical arrows mark the mean (for this date) velocities derived from symmetric absorption lines, $V_r(\text{sym}) \approx -40.1$ km/s, and from short-wavelength components, $V_r(\text{blue}) \approx -60.3$ km/s. The vertical dashed line is the systemic velocity, $V_{\text{sys}} = -47$ km/s [20, 19]. The points show the assumed shape of the wing of the BaII 6141 Å photospheric line in the absence of emission. The position of this lines core in the diagram corresponds to the positions of symmetric moderate-intensity absorption lines in the same spectrum.

calculations were done using the modified STARS code [33], adapted for a Linux environment. According to the data from Table 1, the effective temperature for September 24, 2010 was $T_{\text{eff}} \approx 6000$ K. We took the surface gravity $\log g = 0.1$, microturbulence velocity $\xi_t = 12$ km/s, and slight deviations of the chemical abundances from the solar values from [34]. Theoretical modeling of spectra does not provide the necessary accuracy for extremely luminous stars. However, we did not attempt to accurately reproduce the line intensities, since we were mainly interested in their positions. The position of the theoretical BaII 6141 Å line profile agrees well with the long-wavelength component in the observed spectrum. This provides additional evidence supporting our suggestion that the long-wavelength components of split absorption lines are formed in the same layers of the stellar atmosphere as those where the symmetric, isolated absorption lines are formed. The short-wavelength component clearly originates in the envelope.

Note that splitting of strong absorption lines was detected [35] in the spectrum of the post-AGB supergiant V354 Lac, whose mass and evolutionary stage are very different from those of the hypergiant ρ Cas. Analysis of radial-velocity data from echelle spectra of V354 Lac obtained using the 6-m telescope + the NES spectrograph shows that the strongest absorption

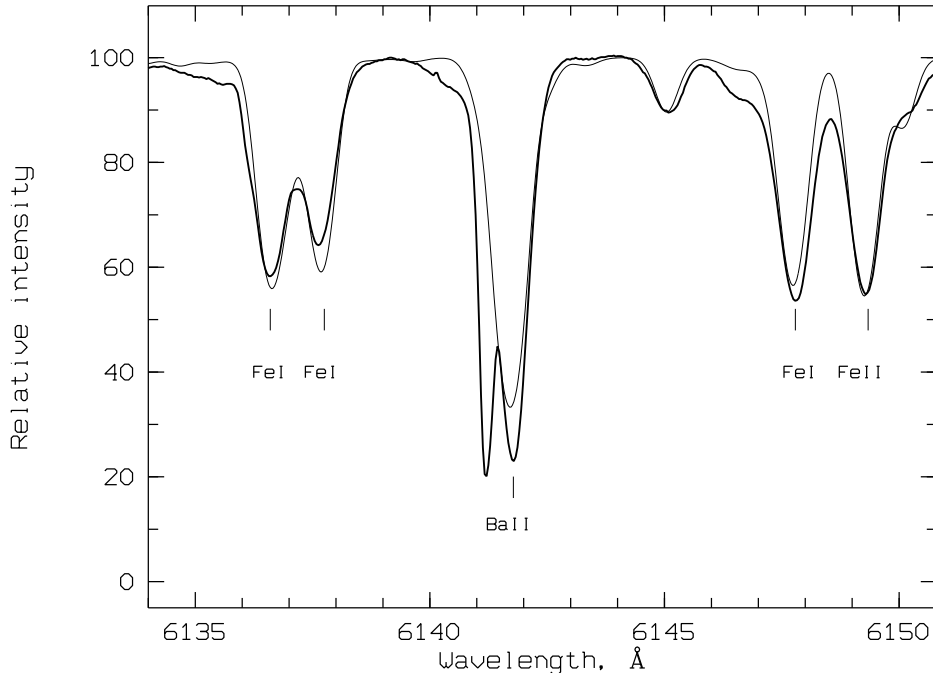


Figure 4. Fragment of the spectrum of ρ Cas obtained on September 24, 2010 (JD 2455654.4; bold curve) compared to the theoretical spectrum computed for $T_{\text{eff}} = 6000$ K, $\log g = 0.1$, microturbulence velocity $\xi_t = 12$ km/s, and macroturbulence velocity $\zeta_t = 20$ km/s (thin curve).

lines of metal ions (BaII, LaII, CeII, NdII) are distorted by a component formed in an envelope expanding at a constant velocity.

Gesicki [36] used photographic spectra of ρ Cas taken by J. Smolinski during 1969–1970 to study the temporal behavior of the BaII 4934, 5853 and FeI 5328 Å lines. The main conclusion of this work was that the short-wavelength component is formed in an expanding circumstellar envelope with a very high gas temperature, ≈ 12000 K. Our results are consistent with this formation region for the short-wavelength component. However, Gesicki [36] concluded from monitoring of a small number of lines that neither component of the split absorption lines varied their velocity V_r during the pulsation period. Our more accurate measurements demonstrate that the positions of both components of the split absorption lines vary in time with an amplitude of several km/s.

Recently, Gorlova et al. [32] suggested a different explanation of the splitting of low-excitation absorption lines observed in spectra of ρ Cas. They suggest that the splitting is due to a stationary emission feature with $V_r \approx -50$ km/s formed in the circumstellar medium, which overlaps with absorption lines broadened by strong turbulence. Their main argument against the hypothesis that the short-wavelength components are formed in the circumstellar medium is that the presence of two independent absorption components would require the continual existence of layers moving both outwards and inwards towards the stellar center, which can be ruled out for physical reasons.

Note that the assumption of oppositely directed motions (compression of some layers and expansion of others) is justified in the 1D model atmosphere if both the zones of compression and expansion have densities and temperatures sufficient to form absorption lines with detectable intensities. In this case, lines due to different ionization states or excitation states can dominate in different zones. If the oppositely directed motions are present in different parts of the observed stellar hemisphere (for example, due to non-symmetric pulsations),

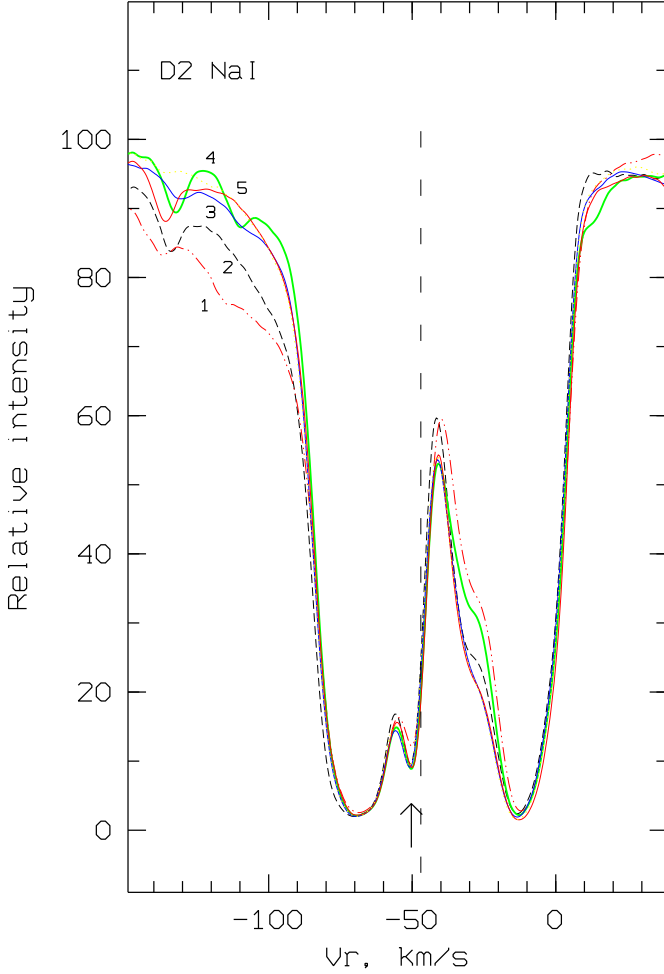


Figure 5. Profile of the D2 NaI line in the spectra of ρ Cas at various epochs: 1 – February 21, 2008; 2 – October 20, 2008; 3 – September 30, 2009; 4 – September 24, 2010; 5 – January 13, 2011. The arrow marks the interstellar component, $V(\text{IS}) \approx -50$ km/s [37]. The vertical dashed line is the systemic velocity, $V_{\text{sys}} = -47$ km/c [20, 19].

the condition for the line components formed in the ascending and descending parts of the hemisphere to be simultaneously detectable is determined by the ratio of the combined areas of the ascending and descending parts and the ratio of the corresponding temperatures (since the contribution to the flux is dependent on the temperature as well as the area).

Our proposed explanation for the observed splitting of the strongest absorption line suggests a simpler pattern for the differential motions: low-amplitude pulsations plus expansion of the upper layers of the extended atmosphere forming a transition to the envelope, plus the presence of velocity gradients in the stellar atmosphere and envelope at some times. Another important difference of our results from those of Lobel et al. [27, 19] or Gorlova et al. [32] is that, using spectra over a wide wavelength range, we have been able to analyze velocities from symmetric absorption lines whose profiles are not distorted by circumstellar features. As a result, the pulsation amplitude we have found, about ± 7 km/s, is half the value derived in [27].

Other lines with anomalies.

In addition to broad components similar to those we see for the strongest absorption lines, the D NaI line profiles (Fig. 5) contain a narrow absorption feature at $V_r = -49.8$ km/s and a component near $V_r \approx -29$ km/s, poorly visible in our spectra. The absorption at $V_r \approx -50$ km/s has an interstellar origin, and corresponds to the location of ρ Cas in the Perseus arm [37]. The interstellar NaI line corresponding to the Local Arm cannot be identified against the long-wavelength photospheric component.

In the spectra s516015 and s538009, we measured an abnormal V_r velocity from the FeII 6369.46 and 6432.68 Å ion lines. When these spectra were obtained, the short-wavelength wings of the two lines, which have the same ionization potential $\chi_{low} = 2.89$ eV, were distorted by emission, especially clearly expressed in the s538009 spectrum. The horizontal arrow in the corresponding panel of Fig. 2 indicates the mean velocity of the emission component of the FeII 6369.46 and 6432.68 Å lines in these spectra, $V_r = -68.4$ km/s. Obviously, these wind emission lines were formed in the same layers as the short-wavelength components of the split metallic absorptions.

In addition to the position measurements for the groups of metal lines noted above, we also present the velocity derived from the absorption components of the H δ , H γ , H β , and H α lines for all the spectra containing neutral-hydrogen lines. The positions of the H δ , H γ , and H β cores, plotted as crosses in Fig. 2, vary between the systemic velocity and the velocity derived from the absorption lines of metal ions (triangles). At some epochs, the position of the H α absorption core (circled cross) also coincides with the systemic velocity, but, more often, this line follows the $V_r(r)$ sequence for the long-wavelength components of split absorption lines.

5. Conclusions

We have derived effective temperatures and radial velocities from spectral features formed in different layers of the extended atmosphere of the hypergiant ρ Cas using 12 high-quality echelle spectra taken during various observing seasons in 2007–2011. The effective temperature of the star varied within 5777–6744 K.

Due to our wide wavelength range, we were able to study the velocity field using an unprecedentedly large number of isolated (several hundred in each spectra) and split (from 12 in the visual to 89 in the short-wavelength range) absorptions. The radial velocity derived from weak, symmetric absorption lines of metals varies from epoch to epoch with an amplitude of about ± 7 km/s relative to $V_{sys} = -47$ km/s, as a consequence of low-amplitude pulsations in the stellar atmosphere. At certain times, we observed a relation between the radial velocity and the line intensity, indicating the presence of a velocity gradient in deep layers of the stellar atmosphere. For several phases, we also found a difference of 3–4 km/s between the velocities measured from absorption lines of neutral atoms and of ions. Thus, we are the first to detect velocity stratification in the atmosphere of ρ Cas.

We demonstrated that the long-wavelength components of the split BaII, SrII, TiII absorptions and of other strong lines with low excitation potentials for their lower levels were distorted by a stationary emission feature, which shifted the line toward longer wavelengths. Thus, the long-wavelength components of the split absorption lines are ordinary absorption features; taking into account the distortion by the stationary emission feature at individual epochs, the formation region and radial velocities of these components do not differ from those for single absorption lines.

The radial velocities of short-wavelength components were reliably determined using a large number of features, and lie in a narrow range from $V_r(\text{blue}) \approx -60$ to -70 km/s. The short-wavelength components of these absorption lines are formed in the circumstellar

envelope, where one component of the D NaI doublet lines and the emission components for the FeII 6369.46 and 6432.68 Å ion lines are also formed.

Acknowledgments

The authors thank Dr. M.V. Yushkin for his great help during the observations. This study was supported by the Russian Foundation for Basic Research (project no. 11-02-00319 a).

References

1. C. de Jager, Ann. Rev. Astron. Astrophys. **8**, 145 (1998).
2. C. de Jager, A. Lobel, H. Nieuwenhuijzen, and R. Stothers, Mon. Not. R. Astron. Soc. **327** 452 (2001).
3. R.M. Humphreys, Rev. Mex. Astron. Astrofis. **30** 6 (2007).
4. Y. Takeda and M. Takada-Hidai, Publ. Astron. Soc. Japan. **46** 395 (1994).
5. Yu.A. Fadeyev, Astron. Lett. **37** 403 (2011).
6. A. Lobel, A.K. Dupree, R.P. Stefanik, et al., Astrophys. J. **583** 923 (2003).
7. H. Nieuwenhuijzen and C. de Jager, Astron. Astrophys. **353** 163 (2000).
8. V. Klochkova, E. Chentsov, and V. Panchuk, Mon. Not. R. Astron. Soc. **292** 19 (1997).
9. R.D. Oudmaijer, Astron. Astrophys. Suppl. Ser. **129** 541 (1998).
10. V.G. Klochkova, M.V. Yushkin, E.L. Chentsov, and V.E. Panchuk, Astron. Rep. **46** 139 (2002).
11. M.T. Schuster, R. M. Humphreys, and M. Marengo, Astron. J. **131** 603 (2006).
12. W.P. Bidelman and A. McKellar, Publ. Astron. Soc. Pacif. **69** 31 (1957).
13. V. Panchuk, V. Klochkova, M. Yushkin, and I. Najdenov, in *UV Astronomy: Stars from Birth to Death*, Proceedings of the Joint Discussion No. 4 during the IAU General Assembly of 2006, Ed. by A.I. Gomez de Castro and M.A. Barstow (Editorial Complutense, Madrid, 2007), p. 179.
14. V.E. Panchuk, V.G. Klochkova, M.V. Yushkin, and I.D. Naidenov, J. Opt. Technology. **76** 42 (2009).
15. M.V. Yushkin and V.G. Klochkova, Preprint Spec. Astrophys. Observ. No. 206 (2005).
16. V.G. Klochkova, V.E. Panchuk, M.V. Yushkin, and D.S. Nasonov, Astrophys. Bull. **63** 386 (2008).
17. V.G. Klochkova and N.S. Tavganskaya, Astrophys. Bull. **65** 18 (2010).
18. V.V. Kovtyukh, Mon. Not. R. Astron. Soc. **378** 617 (2007).
19. A. Lobel, G. Israelian, C. de Jager, et al., Astron. Astrophys. **330** 659 (1998).
20. D.L. Lambert, K.H. Hinkle and D.N.B. Hall, Astrophys. J. **248** 638 (1981).
21. W.L.W. Sargent, Astrophys. J. **134** 1425 (1961).
22. C. de Jager, A. Lobel, and G. Israelian, Astron. Astrophys. **325** 714 (1977).
23. V.G. Gorbatskii, Sov. Astron. **5** 192 (1961).

24. K.V. Bychkov and V.E. Panchuk, *Sov. Astron.* **21** 189 (1977).
25. R.M. Humphreys, K. Davidson, and N. Smith, *Astron. J.* **124** 1026 (2002).
26. R.M. Humphreys, D.W. Strecker, T.L. Murdock, and F.J. Low, *Astrophys. J. Lett.* **179** L49 (1973).
27. A. Lobel, C. de Jager, H. Nieuwenhuijzen, et al., *Astron. Astrophys.* **291** 226 (1994).
28. R.A. Bartaya, K.B. Chargeishvili, E.L. Chentsov, and Z.U. Shkhagosheva, *Bull. Spec. Astrophys. Observ.* **38** 103 (1994).
29. V.G. Klochkova, E.L. Chentsov, N.S. Tavganskaya, and M.V. Shapovalov, *Astrophys. Bull.* **62** 162 (2007).
30. N.E. Piskunov, F. Kupka, T.A. Ryabchikova, et al., *Astron. Astrophys. Suppl. Ser.* **112** 525 (1995).
31. F. Kupka, N.E. Piskunov, T.A. Ryabchikova, et al., *Astron. Astrophys. Suppl. Ser.* **138** 119 (1999).
32. N. Gorlova, A. Lobel, A.J. Burgasser, et al., *Astrophys. J.* **651** 1130 (2006).
33. V.V. Tsymbal, in *Model Atmospheres and Spectrum Synthesis*, ASP Conf. Ser. **108** 198 (1996).
34. Y. Takeda and M. Takada-Hidai, *Publ. Astron. Soc. Jpn.* **50** 629 (1998).
35. V.G. Klochkova, *Astron. Lett.* **35** 457 (2009).
36. K. Gesicki, *Astron. Astrophys.* **254** 280 (1992).
37. Y.P. Georgelin and Y.M. Georgelin, *Astron. Astrophys.* **6** 349 (1970).